Ab Initio and Variational Transition State Approach to β-C_3N_4 Formation: Kinetics for the Reaction of CH_3NH_2 with H

Qingzhu Zhang,[†,‡] R. Q. Zhang,*[,†] K. S. Chan,[†] and I. Bello[†]

Center of Super-Diamond and Advanced Films and Department of Physics and Materials Science, City University of Hong Kong, Hong Kong SAR, China, and Enviroment Research Institute, Shandong University, Jinan 250100, People's Republic of China

Received: June 13, 2005; In Final Form: August 5, 2005

The CH_3NH_2 molecule has been considered as either an important intermediate in methane and ammonia mixtures or a precursor in methylamine and hydrogen mixtures in the synthesis of carbon nitride thin films. The fast Hydrogen (H) abstraction from CH_3NH_2 is an important process involved in the formation of HCN or CNH in the chemical vapor deposition (CVD) of carbon nitride thin films. The energetic and kinetic characteristics of the H abstraction reaction from CH_3NH_2 by atomic H used in CVD of β-C_3N_4 were studied using ab initio direct dynamics methods for the first time. Two primary processes were identified for this reaction: H abstraction from the CH_3 group and H abstraction from the NH_2 group. On the basis of ab initio data, the rate constants of each channel have been deduced by canonical variational transition state theory with small-curvature tunneling correction over a wide temperature range of 200 to ~3000 K. The theoretical results were compared with available experimental data.

Introduction

Since β-C_3N_4 was proposed to be stable and harder than diamond,[1−2] the available hardest material, considerable efforts in the search for this material have been made using various experimental approaches.[3−8] However, experimentalists have faced great difficulties in synthesizing the theoretical CN crystalline phase. No credible evidence yet could demonstrate a successful synthesis of crystalline β-C_3N_4 material. Obviously, to harness a successful synthesis, an insightful understanding of the formation mechanism of carbon nitride materials is highly desirable. Chemical vapor deposition (CVD) is one of the important techniques employed for the synthesis of carbon nitride because of its demonstrated success for the synthesis of other metastable phases such as diamond.[9] CH_4, NH_3, and H_2 are common precursors used in the CVD process to produce carbon nitride thin films. To form carbon nitride films, the C−N bond should be formed at the first step. Therefore, the CH_3NH_2 molecule has been considered as an important intermediate in the synthesis of carbon nitride thin films. Once CH_3NH_2 is formed, in an environment of H atoms, the successive H abstraction processes will react: $CH_3NH_2 + H \rightarrow CH_2NH_2 + H_2$; $CH_3NH_2 + H \rightarrow CH_3NH + H_2$; $CH_2NH_2 + H \rightarrow NH_2CH + H_2$; $CH_2NH_2 + H \rightarrow CH_2NH + H_2$; $NH_2CH + H \rightarrow CHNH + H_2$; $CH_2NH + H \rightarrow CHNH + H_2$; $HNCH + H \rightarrow CNH + H_2$; and $HNCH + H \rightarrow HCN + H_2$. To realize the fundamental mechanisms of carbon nitride formation and offer guidance to experimentalists, we have performed two theoretical studies of the chemical reactions involved in β-C_3N_4 synthesis.[10−11] They are (1) the chemical reactions in a CVD process using CH_4, NH_3, and H_2 as precursors[10] and (2) the ab initio method and RRKM theory study of the mechanism and rate constants for CH_3NH_2 decomposition (because the CH_3NH_2 molecule has been considered as either an important intermediate or direct precursor in carbon nitride synthesis).[11] As an ongoing effort, we theoretically investigate the mechanism and kinetic properties for the reaction of CH_3NH_2 with H, which is expected to be useful for improving carbon nitride deposition.

The important features of the present study are as follows: (1) the energy profile surfaces have been calculated at the QCISD(T)/6-311+G(3df,2p)//MP2/6-311G(2d,2p) theory level; (2) the kinetic nature has been studied in the temperature range from 200 to 3000 K using interpolated canonical variational transition-state theory (CVT)[12−14] and the centrifugal dominant, small-curvature tunneling (SCT)[15] approximation, including information about the reactants, products, transition state, and extra points along the minimum energy path; (3) the non-Arrhenius expressions have been fitted; and (4) the calculated rate constants are compared with the available experimental values.

Computational Methods

High-level ab initio calculations have been carried out for the reaction of CH_3NH_2 with H using the Gaussian 98 package.[16] In this paper, MP2 and QCISD(T) denote the unrestricted versions, UMP2 and UQCISD(T). The geometrical parameters of the reactant, transition states, and products have been optimized at the MP2/6-311G(2d,2p) level. The vibrational frequencies have been calculated at the same level to determine the nature of the stationary points, the zero-point energy (ZPE), and the thermal contributions to the free energy of activation. Each transition state was verified to connect the designated reactants and products by performing an intrinsic reaction coordinate (IRC) analysis. At the MP2/6-311G(2d,2p) level, the minimum energy paths (MEP) were constructed, starting from the transition state geometries and going downhill to both the asymptotic reactant and the product channel with a gradient step size of 0.02 $amu^{1/2}$ bohr, for all the channels. The force constant matrixes of the stationary points and selected nonstationary points near the saddle point along the MEP were also calculated. Although the geometrical parameters and frequencies of various

* Corresponding author. E-mail: aprqz@cityu.edu.hk.
[†] City University of Hong Kong.
[‡] Shandong University.

10.1021/jp0531661 CCC: $30.25
Published on Web 09/17/2005

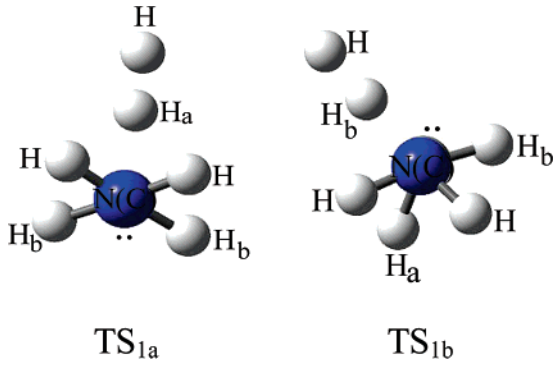

Figure 1. Structures of the transition states TS_{1a} and TS_{1b} for H abstraction from the CH_3 group.

species can be determined satisfactorily at the MP2/6-311G-(2d,2p) level, the energies obtained at this level may not be accurate enough for the subsequent kinetics calculations. Therefore, a higher level, QCISD(T), and a more flexible basis set, 6-311+G(3df,2p), were employed to determine the energies of various species.

The initial information obtained from our ab initio calculations allowed us to calculate the variational rate constant including the tunneling effect contribution. The canonical variational theory (CVT) rate constant[12−14] for temperature T is given as

$$k^{\mathrm{CVT}}(T,s) = \min k^{\mathrm{GT}}(T,s) \tag{1}$$

where

$$k^{\mathrm{GT}}(T,s) = \frac{\sigma k_{\mathrm{B}} T}{h} \frac{Q^{\mathrm{GT}}(T,s)}{\Phi^{\mathrm{R}}(T)} \mathrm{e}^{-V_{MEP}(s)/k_B T} \tag{2}$$

<noparaPwhere $k^{\mathrm{GT}}(T,s)$ is the generalized transition state theory rate constant at the dividing surface s, σ is the symmetry factor accounting for the possibility of more than one symmetry-related reaction path, k_{B} is the Boltzmann constant, h is Planck's constant, $\phi^{\mathrm{R}}(T)$ is the reactant partition function per unit volume, excluding symmetry numbers for rotation, and $Q^{\mathrm{GT}}(T,s)$ is the partition function of a generalized transition state at s with a local zero energy at $V_{\mathrm{MEP}}(s)$ and with all rotational symmetry numbers set to unity. The minimum energy path (MEP) was obtained at the MP2/6-311G(2d,2p) level by the IRC definition, and the classical potential energies $V_{\mathrm{MEP}}(s)$ were refined by the QCISD(T)/6-311+G(3df,2p)//MP2/6-311G(2d,2p) method. All kinetics calculations have been carried out using the POLYRATE 9.3 program.[17] The rotational partition functions were calculated classically, and the vibrational modes were treated as quantum-mechanical separable harmonic oscillators.

Results and Discussion

The optimized geometries of the reactants, transition states, and products are shown in Figures 1 and 2 for the reaction of CH_3NH_2 with H. The vibrational frequencies of the reactants, products, and transition states are listed in Table 1. The calculated classical potential barriers ΔE and the reaction enthalpies ΔH are summarized in Table 2. Figure 3 shows the classical potential energy (V_{MEP}) and vibrationally adiabatic potential energy (V_a^{G}) curves as functions of distance along the reaction coordinate s at the QCISD(T)/6-311+G(3df,2p)//MP2/6-311G(2d,2p) level for the channel of H abstraction from NH_2 group. The changes in the curves of generalized normal-mode vibrational frequencies with the reaction coordinate s are shown in Figure 4 for the channel of H abstraction from the NH_2 group. The calculated total CVT/SCT rate constants along with the experimental values are presented in Figure 5 in the temperature range of 200 to ~3000 K. The calculated branching ratios as a function of the reciprocal of the temperature (T) are shown in Figure 6 for the temperature range of 200 to ~3000 K and for each channel. The calculated TST, CVT, and CVT/SCT rate constants as a function of the reciprocal of the temperature (T) in the temperature range of 200 to ~3000 K for the channel of H abstraction from CH_3 group via transition state TS_{1a} are signified in Figure 7. Figure 8 shows the TST and CVT rate constants with different tunneling contributions.

Reaction Mechanism. To clarify the general reliability of the theoretical calculations, it is useful to compare the predicated chemical properties of the present particular systems of interest with experimental data. As shown in Figure 1, the geometric parameters of CH_3NH_2 optimized at the MP2/6-311G(2d,2p) level are in good agreement with the available experimental values,[18−19] and the maximum relative error of the bond length is less than 0.5%. As can be seen from Table 1, the vibrational frequencies of CH_3NH_2 predicated from the MP2/6-311G-(2d,2p) calculations agree well with the experimentally observed fundamentals,[18−19] and the maximum relative error is less than 8.0%, except for the four smallest frequencies (the maximum relative error is more than 10.0%). For comparison, in addition to the MP2/6-311G(2d,2p) method, the geometric parameters and vibrational frequencies were also computed at the B3LYP/6-31G(d) levels of theory. As shown in Figure 1, the maximum relative error of the bond length obtained at B3LYP/6-31G(d) is 1.0% as compared with the available experimental values. The frequencies calculated at MP2 and B3LYP do not show a great change. The energies of all the species are calculated at the QCISD(T)/6-311+G(3df,2p)//MP2/6-311G(2d,2p), G3B3//B3LYP/6-31G(d), and G2MP2-B3//B3LYP/6-31G(d) levels. As shown in Table 2, the potential barriers obtained at QCISD(T)/6-311+G(3df,2p)//MP2/6-311G(2d,2p) including the ZPE correction are in agreement with the results calculated at the G3B3//B3LYP/6-31G(d) level. The G3B3//B3LYP/6-31G(d) level predicts lower barrier heights for all the channels. The QCISD-(T)/6-311+G(3df,2p)//MP2/6-311G(2d,2p) level is more expensive than the G3B3//B3LYP/6-31G(d) and G2MP2-B3//B3LYP/6-31G(d) levels. Therefore, the geometrical parameters and frequencies calculated at the MP2/6-311G(2d,2p) level and the energies obtained at the QCISD(T)/6-311+G(3df,2p) level are used for the following mechanism and kinetics calculation.

The reaction of CH_3NH_2 with atomic H is a prototype of a simple metathesis reaction in which a hydrogen atom is transferred via an apparent barrier in the reaction coordinate. Two primary processes have been identified:

$$CH_3NH_2 + H \rightarrow CH_2NH_2 + H_2 \quad R_1$$

H abstraction from the CH_3 group

$$CH_3NH_2 + H \rightarrow CH_3NH + H_2 \quad R_2$$

H abstraction from the NH_2 group

H Abstraction from the CH_3 Group. Reactant CH_3NH_2 has C_s symmetry. Three hydrogen atoms bonded with the C atom are unequivalent. The H atom (denoted as H_a) in the symmetry plane is different from the other atoms (denoted as H_b). As a result, two transitions states, TS_{1a} and TS_{1b}, were found for the H abstraction from the CH_3 group. Thus, the H abstraction from the CH_3 group via TS_{1a} and TS_{1b} are described as reactions R_{1a} and R_{1b}. The reaction path symmetry numbers are 1 for reaction R_{1a} and 2 for reaction R_{1b}. The structures of the transition states

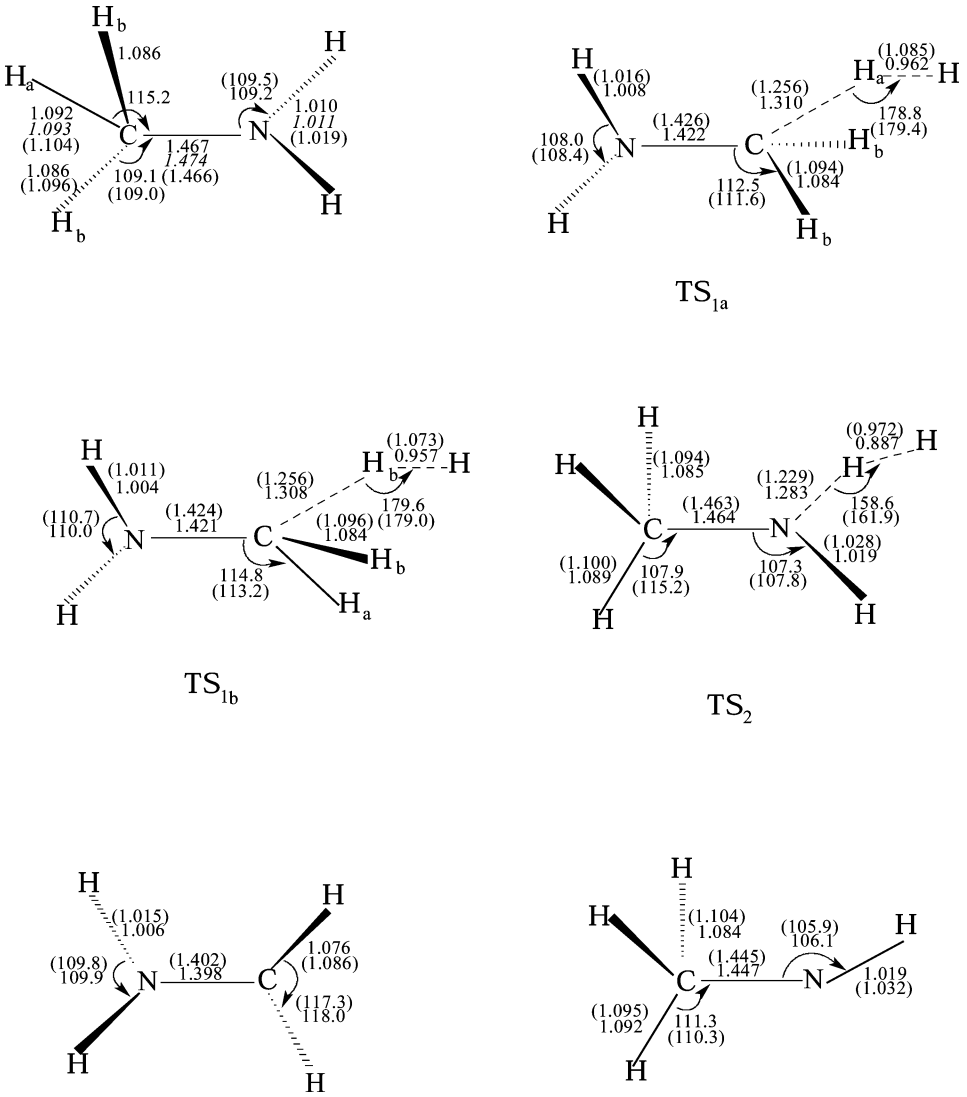

Figure 2. Optimized geometrical parameters at the MP2/6-311G(2d,2p) level for the reactant, products, and transition states involved in the reaction of CH_3NH_2 and H. Distances are in angstroms, and angles are in degrees. The values in parentheses are the results obtained at the B3LYP/6-31G(d) level, and the values in italics are the experimental data.[18−19]

TABLE 1: Calculated Vibrational Frequencies (in cm^{-1}) for the Reactant, Products, and Transition States Involved in the Reaction of CH_3NH_2 with H at the MP2/6-311G(2d,2p) Level[a]

species	frequencies									
CH_3NH_2	3631	3549	3171	3134	3045	1684	1553	1533	1485	1376
	1204	1073	991	890	316					
	*3549	3465	3119	3079	2972	1704	1547	1528	1485	1373
	1194	1069	989	880	336					
	3427	*3361*	*2985*	*2961*	*2820*	*1623*	*1485*	*1473*	*1430*	*1335*
	1130	*1195*	*1044*	*780*	*268*					
CH_2NH_2	3699	3595	3314	3196	1674	1516	1357	1230	965	770
	680	480								
CH_3NH	3481	3174	3091	3034	1523	1520	1438	1369	1062	1022
	977	260								
H_2	4530									
TS_{1a}	3667	3573	3218	3128	1684	1502	1496	1391	1329	1319
	1177	1099	1001	815	566	341	297	1811i		
TS_{1b}	3724	3621	3211	3117	1676	1522	1499	1383	1324	1315
	1161	1102	995	637	520	327	95	1898i		
TS_2	3484	3177	3134	3065	1973	1539	1514	1459	1400	1292
	1149	1055	1006	992	749	400	194	2107i		

[a] The data with and asterisk are the values obtained at the B3LYP/6-31G(d) level, and the values in italics are the experimental data.[18−19]

TS_{1a} and TS_{1b} are depicted in Figure 1, and the optimized geometrical parameters at the MP2/6-311G(2d,2p) level for the transition states TS_{1a} and TS_{1b} are shown in Figure 2. The transition state TS_{1a} has C_s symmetry, and TS_{1b} has C_1 symmetry. The reactive C−H, being broken, is elongated by 19.96 and 20.44%, while the formed H−H bond is longer than the equilibrium value of 0.736 Å in H_2 by 30.71 and 30.02%

TABLE 2: Calculated Classical Potential Barriers ΔE (in kcal/mol) and the Reaction Enthalpies ΔH (in kcal/mol) at the QCISD(T)/6-311+G(3df,2p)//MP2/6-311G(2d,2p) Level for All Channels Involved in the Reaction of CH_3NH_2 with H

energy	R_{1a}	R_{1b}	R_2
ΔE	7.97	11.06	12.06
	(6.49)	(9.05)	(10.55)
	6.36[a]	8.81[a]	10.77[a]
	4.53[b]	6.99[b]	8.29[b]
ΔH	−8.96	−8.96	−6.58
	(−11.29)	(−11.29)	(−9.66)
	−11.93[a]	−11.93[a]	−5.53[a]
	−14.25[b]	−14.25[b]	−8.15[b]

[a] The results obtained at the G3B3 level on the standard B3LYP/6-31G(d) geometry. [b] The values obtained at the G2MP2-B3 level on the standard B3LYP/6-31G(d) geometry. The values in parentheses are obtained at the QCISD(T)/6-311+G(3df,2p)//MP2/6-311G(2d,2p) level including the ZPE correction.

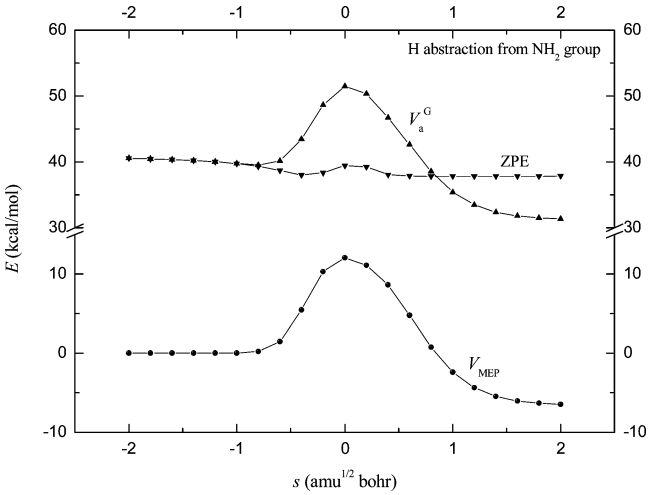

Figure 3. Classical potential energy (V_{MEP}) and vibrationally adiabatic potential energy (V_a^G) curves as functions of s at the QCISD(T)/6-311+G(3df,2p)//MP2/6-311G(2d,2p) level for the channel of H abstraction from the NH_2 group.

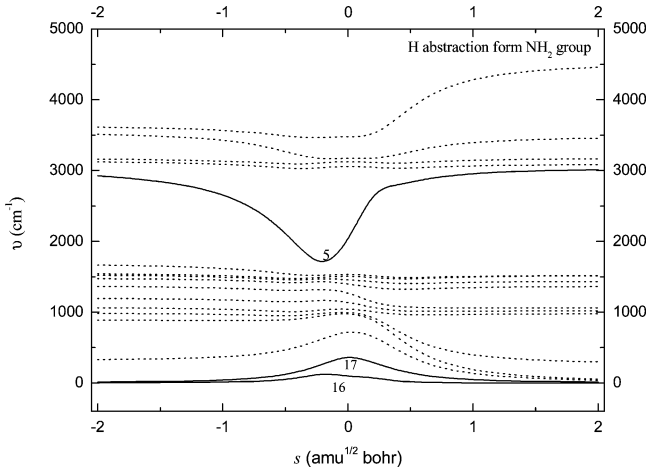

Figure 4. Changes of the generalized normal-mode vibrational frequencies as functions of s at the MP2/6-311G(2d,2p) level for the channel of H abstraction from the NH_2 group.

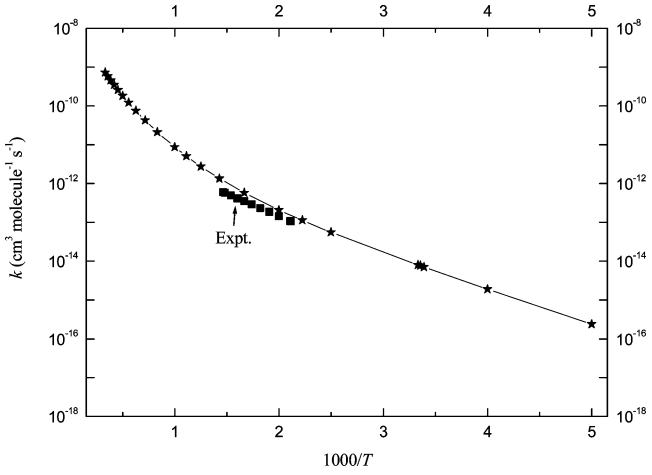

Figure 5. Total CVT/SCT rate constants along with the experimental values in the temperature range of 200−3000 K for the reaction of CH_3NH_2 with H.

for the transition states TS_{1a} and TS_{1b}, respectively. Therefore, these two transition states are reactant-like, and the H abstraction reaction from the CH_3 group proceeds via early transition states. This rather early character in these transition states

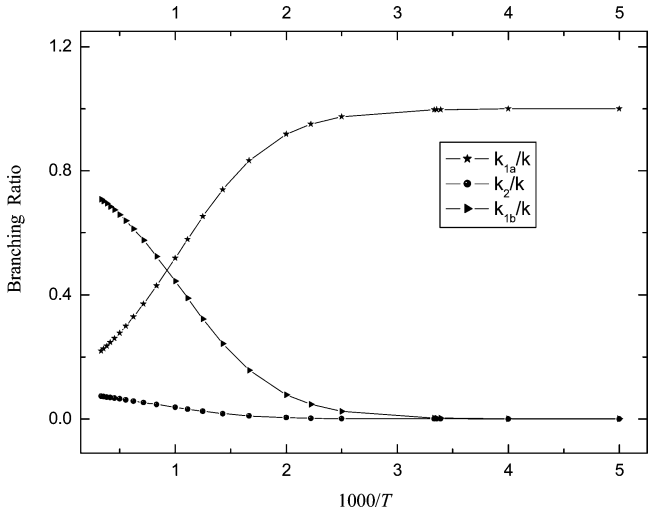

Figure 6. Branching ratios as functions of the reciprocal of the temperature (T) over the temperature range of 200 to ~3000 K for all channels including the reaction of CH_3NH_2 with atomic H.

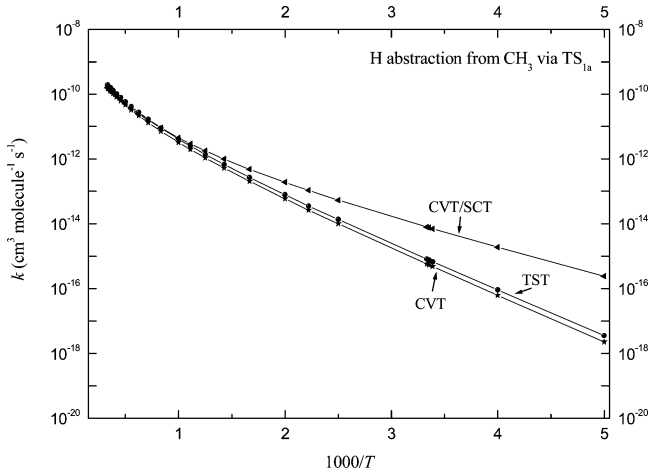

Figure 7. TST, CVT, and CVT/SCT rate constants in the temperature range of 200−3000 K for the channel of H abstraction from the CH_3 group via the transition state TS_{1a}.

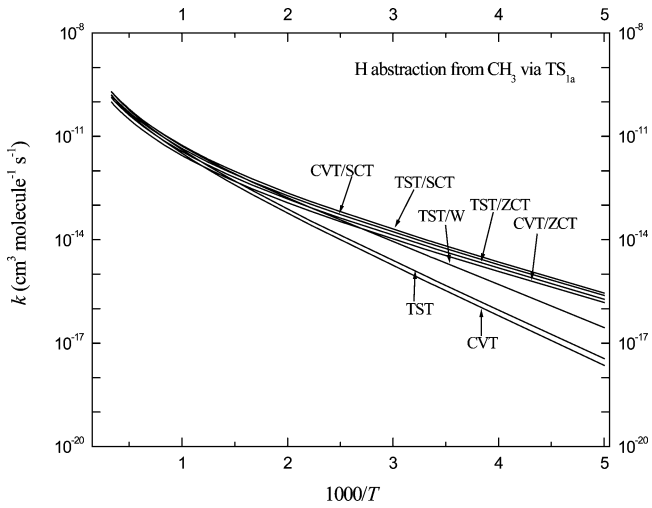

Figure 8. TST and CVT rate constants with Wigner tunneling, ZCT, and SCT contributions in the temperature range of 200−3000 K for the channel of H abstraction from the CH_3 group via the transition state TS_{1a}.

is in accordance with the low reaction barrier and high exothermicity of these two channels, in conformity with Hammond's postulate.[20]

Each transition state is identified with one negative eigenvalue of the respective Hessian matrix and, therefore, one imaginary frequency. Since the imaginary frequency governs the width of the classical potential energy barrier along MEP, it plays an important role in the tunneling calculations, especially when the imaginary frequency is large and the associated eigenvector has a large component of hydrogenic motion. For the two channels of H abstraction from the CH_3 group, the imaginary frequencies of TS_{1a} and TS_{1b} are 1811i and 1898i, so we expect that the tunneling effect should be important for the calculation of the rate constant. It can be seen from Table 2 that the channel R_{1a} is more exothermic and has a lower barrier height as compared to the channel R_{1b}. At the QCISD(T)/6-311+G(3df,2p)//MP2/6-311G(2d,2p) level, the barrier height of 7.97 kcal/mol for channel R_{1a} is lower than that of channel R_{1b} by 3.09 kcal/mol. This implies that the hydrogen abstraction from the CH_3 group via the transition state TS_{1a} is easier than via the transition state TS_{1b}. The difference between the transition states TS_{1a} and TS_{1b} can be analyzed by the changes in the electron density distribution due to the unbonded P-electron pair (denoted as "••" in Figure 1) in the N atom. Because of the high electronegativity of the unbonded P-electron pair, the electron density on the H_a atom is higher than that on other two H_b atoms. The electron density redistribution leads to lowering the polarization of the $C-H_a$ bond and makes it easier to break. Similarly, the net electron redistribution caused by the filled p-orbital in the N atom results in stronger $C-H_b$ bonds. Therefore, the barrier height is lower for channel R_{1a} than for R_{1b}, and as a result, channel R_{1a} is preferred at lower temperatures.

H Abstraction from the NH_2 Group. Since the two hydrogen atoms bonded with the N atom are degenerated in the reactant CH_3NH_2, only one transition state (denoted as TS_2) was located for the channel of the H abstraction from the NH_2 group. At the MP2/6-311G(2d,2p) level, the breaking C−H bonds are elongated by 27.03%, while the forming H−H bonds are longer than the equilibrium value of 0.736 Å by 20.52%. This result indicates that the barrier of the hydrogen abstraction from the NH_2 group is almost centrally located. The imaginary frequency of transition state TS_2 is 2107i. This means that the tunneling effect should play an important role in the calculation of the rate constant. At the QCISD(T)/6-311+G(3df,2p)//MP2/6-311G(2d,2p) level, the potential barrier of H abstraction from the NH_2 group is 4.09 kcal/mol higher than that of channel R_{1a} and 1.00 kcal/mol than that of channel R_{1b}. This means that the abstraction of an H atom connected to a C atom of CH_3NH_2 is relatively easier than that connected to N of CH_3NH_2. This view is further evidenced in the following study of the rate constants.

Kinetics Calculation. Reaction Path Properties. The minimum energy path (MEP) for each reaction channel was obtained at the MP2/6-311G(2d,2p) level by the IRC definition with a step size of 0.02 amu$^{1/2}$ bohr, and the energies of MEP were refined by the QCISD(T)/6-311+G(3df,2p)//MP2/6-311G(2d,2p) method. For all channels, the maximum position of the classical potential energy V_{MEP} curve at the QCISD(T)/6-311+G(3df,2p)//MP2/6-311G(2d,2p) level corresponds to the saddle point structure at the MP2/6-311G(2d,2p) level. Therefore, the shifting of the maximum position for the V_{MEP} curve caused by the computational technique is avoided (avoiding artificial variational effects).[21] The classical potential energy V_{MEP}, the ground-state vibrational adiabatic potential energy V_a^G, and the zero-point energy (ZPE), where $V_a^G = V_{MEP} + ZPE$, as functions of the reaction coordinate s are plotted in Figure 3 for the channel of H abstraction from the NH_2 group. The V_{MEP} and V_a^G curves are similar in shape, and their maximum positions are almost identical. The zero-point energy ZPE curve is nearly unchanged during the reaction process. This means that the variational effect will be small for the calculation of the rate constant. A similar conclusion can be drawn for the H abstraction channel from the CH_3 group. To analyze this behavior in more detail, we show the variations of generalized normal mode vibrational frequencies along MEP in Figure 4 for the H abstraction from the NH_2 group.

In the negative limit of s, the frequencies are associated with the reactants, while in the positive limit of s, the frequencies are associated with the products. For the sake of clarity, the vibrational frequencies can be divided into three types: (i) spectator modes, (ii) transitional modes, and (ii) reactive modes. The spectator modes have little change or sometimes remain basically unchanged in going from reactants to the saddle point. The transitional modes appear along the reaction path as a consequence of the transformation from free rotation or free translation within the reactant or the product limit into real vibrational motions in the global system. Their frequencies tend to be zero at the reactant and the product limit and reach their maximum in the saddle point zone. The reactive modes are those that undergo the largest change in the saddle point zone, and therefore, they must be related to the breaking/forming of bonds. For the channel of H abstraction from the NH_2 group, the mode 5 that connects the frequency of the N−H stretching vibration of the reactant with the frequency of the H−H stretching vibration of H_2 is the reactive mode. The two lowest vibrational frequencies (modes 16 and 17) are transitional modes, and other modes are spectator modes. From $s = -1.0$ to $s = 1.0$ amu$^{1/2}$ bohr, the reactive modes drop dramatically, and this behavior is similar to that found in other hydrogen abstraction reactions.[22−24] If changes in other frequencies were small, this drop could cause a considerable fall in the zero-point energy near the saddle point, but the drop of the reactive mode compensates the transitional modes. As a result, the zero-point energy ZPE curve is nearly unchanged during the reaction process for the channel of H abstraction from the NH_2 group. Because of the same reason, the classical potential energy V_{MEP} and the ground-state vibrational adiabatic potential energy V_a^G curves are similar in shape to the channel of H abstraction from CH_3 group.

Rate Constant. The canonical variational transition state theory (CVT) with a small-curvature tunneling (SCT) correction that has been successfully performed for several analogous reactions[25−27] is an efficient method to calculate the rate constant. In this paper, we used this method to calculate the rate constants for the reaction of CH_3NH_2 with H over a wide temperature range from 200 to 3000 K. To calculate the rate constant, 30 points were selected near the saddle point along MEP, 15 points were selected in the reactant zone, and 15 points were selected in the product zone. The CVT/SCT rate constants of channels R_{1a} and R_{1b} are noted as k_{1a} and k_{1b}. The rate constants of H abstraction from the NH_2 groups are designated as k_1 and k_2, respectively. The total rate constants of the reaction of CH_3NH_2 with H are assigned as k, $k = k_{1a} + k_{1b} + k_2$. The branching ratios of the channels of H abstraction from the CH_3 and NH_2 groups are ascribed as k_{1a}/k, k_{1b}/k, and k_2/k, respectively.

The total CVT/SCT rate constant, which is the sum of the CVT/SCT rate constants for all the channels, along with the experimental values as a function of the reciprocal of the temperature (T) are in Figure 5. Evidently, the total CVT/SCT rate constants are in good agreement with the experimental values[28] over the temperature range of 473 to ~683 K. Therefore, the CVT/SCT rate constants are taken as the accurate

rate constants for each channel. The calculated rate constants exhibit typical non-Arrhenius behavior. The total CVT/SCT rate constants are fitted by three-parameter formulas over the temperature range of 200−3000 K and given in units of cm^3 $molecule^{-1}$ s^{-1} as follows: $k(T) = (1.34 \times 10^{-21})T^{3.44} \exp(-1223.27/T)$.

The calculated branching ratios as a function of the reciprocal of the temperature (T) over the temperature range of 200 to ~3000 K for each channel are shown in Figure 6. Because of having a smaller potential barrier, H abstraction from the CH_3 group via the transition state TS_{1a} is the dominant reaction channel over the lower temperature range of 200−1000 K. However, as the temperature increases, H abstraction from the CH_3 group via transition state TS_{1b} becomes a competitive reaction channel. Owing to the highest barrier height, the contribution of H abstraction from NH_2 group is minor over the whole temperature range.

To compare further the CVT/SCT rate constants with the conventional transition state theory TST and CVT rate constants, Figure 7 shows the calculated TST, CVT, and CVT/SCT rate constants against the reciprocal of the temperature for the channel of H abstraction from the CH_3 group via transition state TS_{1a}. For the comparison of the tunneling contribution, Figure 8 shows the TST and CVT rate constants using different tunneling effects. Important features of the calculated rate constants are as follows: (1) the values of TST rate constants and CVT rate constants are nearly identical, which enables us to conclude that the variational effect is small for the calculation of the rate constants. This summary is in good agreement with the previous analysis. The same conclusion can be drawn from the other channels. (2) Reactions involving hydrogen atom transfer are usually characterized by significant tunneling effects that must be accounted for in computing reaction rate constants. In the present case, the CVT/SCT rate constants are greater than the CVT ones in the temperature range of 200−800 K; for example, at 298 K, the CVT rate constant is 5.36×10^{-16} cm^3 $molecule^{-1}$ s^{-1}, while the CVT/SCT rate constant is 7.59×10^{-15} cm^3 $molecule^{-1}$ s^{-1}. The latter is 14.16 times larger than the former. However, the difference between the CVT rate constant and the CVT/SCT rate constant decreases with increasing the temperature. When the temperature is higher than 800 K, the CVT/SCT rate constants are asymptotic to the rate constants of CVT, which means that only in the lower temperature range does the small curvature tunneling correction play an important role for the calculation of the rate constant. The same conclusion can be deemed from the channels of R_{1b} and R_2. (3) Figure 8 shows the TST and CVT rate constants with different tunneling methods, the Wigner tunneling (W) method, the zero-curvature tunneling (ZCT) method, and the SCT method, for the channel of H abstraction from the CH_3 group via transition state TS_{1a}. It can be seen from Figure 8 that the choice of the tunneling method has an important effect on the calculation of the rate constants. The Wigner method obtains the smallest transmission coefficients and the samllest reaction-path curvature. The rate constants with a ZCT tunneling contribution are asymptotic to the rate constants using SCT correction, which means that the ZCT method is also efficient for the channel.

Conclusion

In this paper, we study the reaction of CH_3NH_2 with H using the ab initio and canonical variational transition state theory (CVT) with tunneling effects. Rate constants were reported in the temperature range of 200−3000 K. From this calculation, several conclusions can be drawn as follows: (1) the reaction involves three channels: two for H abstraction from the CH_3 group and one for H abstraction from the NH_2 group. At lower temperatures, hydrogen abstraction from the CH_3 group via transition state TS_{1a} is the dominant channel. With an increase in temperature, hydrogen abstraction from the CH_3 group via the transition state TS_{1b} becomes a competitive channel. (2) The variational effect is small for all the channels. (3) The tunneling contribution plays an important role for the calculation of the rate constants in the low-temperature range. (4) The CVT/SCT overall rate constant is consistent with the experimental values in the temperature range of 473−683 K.

Acknowledgment. The work described in this paper is supported by a grant from the Research Grants Council of Hong Kong SAR (Project CityU 2/04C). The authors thank Prof. Donald G. Truhlar for providing the POLYRATE 9.3 program.

References and Notes

(1) Liu, A. Y.; Cohen, M. L. *Science* **1989**, *245*, 841.
(2) Liu, A. Y.; Cohen, M. L. *Phys. Rev. B* **1990**, *41*, 10727.
(3) Niu, C.; Lu, Y. Z.; Lieber, C. M. *Science* **1993**, *261*, 334.
(4) Maya, L.; Cole, D. R.; Hagaman, E. W. *J. Am. Ceram. Soc.* **1991**, *7*, 1686.
(5) Martin-Gil, J.; Martin-Gil, F. J.; Sarikaya, M.; Qian, M.; Yacaman, M. J.; Rubio, A. *J. Appl. Phys.* **1997**, *81*, 2555.
(6) Guo, L. P.; Chen, Y.; Wang, E. G.; Li, L.; Zhao, Z. X. *Chem. Phys. Lett.* **1997**, *268*, 26.
(7) Yu, K. M.; Cohen, M. L.; Haller, E. E.; Hansen, W. L.; Liu, A. Y.; Wu, I. C. *Phys. Rev. B* **1994**, *49*, 5034.
(8) Marton, D.; Boyd, K. J.; Al-Bayati, A. H.; Todorov, S. S.; Rabalais, J. W. *Phys. Rev. Lett.* **1994**, *73*, 118.
(9) Jiang, X.; Klages, C. P. *Diamond Relat. Mater.* **1993**, *2*, 1112.
(10) Zhu, R. S.; Zhang, R. Q.; Chan, K. S. *Chem. Phys. Lett.* **2000**, *320*, 561.
(11) Zhang, R. Q.; Han, K. L.; Zhu, R. S.; Lee, C. S.; Lee, S. T. *Chem. Phys. Lett.* **2000**, *321*, 101.
(12) Baldridge, M. S.; Gordor, R.; Steckler; Truhlar, D. G. *J. Phys. Chem.* **1989**, *93*, 5107.
(13) Gonzalez-Lafont, A.; Truong, T. N.; Truhlar, D. G. *J. Chem. Phys.* **1991**, *95*, 8875.
(14) Garrett, B. C.; Truhlar, D. G. *J. Phys. Chem.* **1979**, *83*, 1052.
(15) Liu, Y. P.; Lynch, G. C.; Truong, T. N.; Lu, D. H.; Truhlar, D. G.; Garrett, B. C. *J. Am. Chem. Soc.* **1993**, *115*, 2408.
(16) Frisch, M. J.; Trucks, G. W.; Schlegel, H. B.; Scuseria, G. E.; Robb, M. A.; Cheeseman, J. R.; Zakrzewski, V. G.; Montgomery, J. A., Jr.; Stratmann, R. E.; Burant, J. C.; Dapprich, S.; Millam, J. M.; Daniels, A. D.; Kudin, K. N.; Strain, M. C.; Farkas, O.; Tomasi, J.; Barone, V.; Cossi, M.; Cammi, R.; Mennucci, B.; Pomelli, C.; Adamo, C.; Clifford, S.; Ochterski, J.; Petersson, G. A.; Ayala, P. Y.; Cui, Q.; Morokuma, K.; Malick, D. K.; Rabuck, A. D.; Raghavachari, K.; Foresman, J. B.; Cioslowski, J.; Ortiz, J. V.; Baboul, A. G.; Stefanov, B. B.; Liu, G.; Liashenko, A.; Piskorz, P.; Komaromi, I.; Gomperts, R.; Martin, R. L.; Fox, D. J.; Keith, T.; Al-Laham, M. A.; Peng, C. Y.; Nanayakkara, A.; Gonzalez, C.; Challacombe, M.; Gill, P. M. W.; Johnson, B.; Chen, W.; Wong, M. W.; Andres, J. L.; Gonzalez, C.; Head-Gordon, M.; Replogle, E. S.; Pople, J. A. *Gaussian 98*, Revision A.7; Gaussian, Inc.: Pittsburgh, PA, 1998.
(17) Steckler, R.; Chuang, Y. Y.; Fast, P. L.; Corchade, J. C.; Coitino, E. L.; Hu, W. P.; Lynch, G. C.; Nguyen, K.; Jackells, C. F.; Gu, M. Z.; Rossi, I.; Clayton, S.; Melissas, V.; Garrett, B. C.; Isaacson, A. D.; Truhlar, D. G. *POLYRATE Version 9.3*; University of Minnesota: Minneapolis, MN, 2002.
(18) Hamado, H. et al. *J. Mol. Spectrosc.* **1982**, *96*, 313.
(19) Oda, M.; Ohashi, N.; Hougen, J. T. *J. Mol. Spectrosc.* **1990**, *142*, 57.
(20) Hammmond, G. S. *J. Am. Chem. Soc.* **1955**, *77*, 334.
(21) Espinosa-Garcia, J.; Corchado, J. C. *J. Phys. Chem.* **1995**, *99*, 8613.
(22) Truhlar, D. G.; Isaacson, A. D. *J. Chem. Phys.* **1982**, *77*, 3516.
(23) Corchado, J. C.; Espinosa-Garcia, J. *J. Chem. Phys.* **1997**, *106*, 4013.
(24) Espinosa-Garcia, J.; Corchado, J. C. *J. Phys. Chem.* **1996**, *100*, 16561.
(25) Zhang, Q.-Z.; Zhang, D.-J.; Wang, S.-K.; Gu, Y.-S. *J. Phys. Chem. A* **2002**, *106*, 122.
(26) Yu, Y. X.; Li, S. M.; Xu, Z. F.; Li, Z. S.; Sun, C. C. *Chem. Phys. Lett.* **1999**, *302*, 281.
(27) Melissas, V. S.; Truhlar, D. G. *J. Chem. Phys.* **1993**, *99*, 1013.
(28) Blumenberg, B.; Wagner, H. G. *Ber. Bunsen-Ges. Phys. Chem.* **1973**, *77*, 253.